Coherent {001} interfaces between rocksalt and zinc-blende crystal structures

H. Groiss, G. Hesser, W. Heiss, and F. Schäffler*
Institut für Halbleiter- und Festkörperphysik, Johannes Kepler Universität, 4040 Linz, Austria

R. Leitsmann and F. Bechstedt
Institut für Festkörpertheorie und- optik, Friedrich Schiller Universität, 07737 Jena, Germany

K. Koike and M. Yano
Osaka Institute of Technology, Asahi-ku Ohmiya, Osaka 535-8585, Japan
(Received 21 April 2009; published 25 June 2009)

We study coherent, two-dimensional (2D) *rocksalt* PbTe epilayers in a *zinc-blende* CdTe matrix. The embedded material transforms during an annealing step into highly symmetric quantum dots with coherent interfaces. The atomic structure of the polar {001} interfaces between the two tellurides is investigated by high-resolution transmission electron microscopy in combination with multislice simulations. Both the original 2D PbTe epilayers and the resulting PbTe quantum dots are terminated by distinctively different cation-terminated [(001)A] and anion-terminated [(001)B] interfaces at opposite faces, whereas for the structurally similar ErAs/InGaAs heterosystem as yet only the (001)A interface was reported in the literature. *Ab initio* simulations were performed to assess these seeming differences, which were found to be mainly caused by the different polar bonding character of the involved II-VI and III-V compounds.

DOI: 10.1103/PhysRevB.79.235331 PACS number(s): 68.65.−k, 68.37.Lp, 68.35.Ct

Heterostructures are often associated with coherent layer sequences of different materials with the same lattice type but not necessarily with the same lattice constant. Less common are coherent heterostructures that combine materials of different lattice type but with similar or almost identical lattice constants. A prototypal example for the latter type consists of the semimetallic monopnictide ErAs, which crystallizes in the rocksalt (*rs*) structure, and the zinc-blende (*zb*) semiconductor $In_{1-x}Ga_xAs$.[1–3] Perfect lattice-constant matching becomes possible via the composition x. Epitaxial-growth conditions and the structural properties of this heterosystem have been investigated intensely, in particular, with respect to the initially forming coherent ErAs nanocrystals on $In_{1-x}Ga_xAs$.[4–6]

Recently, the application potential of lattice-type mismatched heterostructures was greatly expanded with the demonstration of coherently embedded quantum dots (QDs) of the narrow band-gap *rs*-type semiconductor PbTe in a matrix of the *zb*-type wide-gap material CdTe.[7] The PbTe QDs show intense midinfrared photoluminescence at room temperature, which significantly exceeds that of bulk PbTe due to carrier confinement in the QDs.[8] Near thermal equilibrium the PbTe QDs assume the shape of rhombocubo-octahedrons,[7–9] which are terminated by {100}, {110}, and {111} faces, as shown in Fig. 1(a). In Ref. 9 high-resolution transmission electron microscopy (HRTEM) and first-principles total-energy calculations in the repeated slab approximation were combined to quantitatively determine the structural arrangements of the {110} interface on an atomic level. The {110} interface is the least complex of the three interfaces because the {110} plane is neutral in both CdTe and PbTe. Still, the coordination mismatch at the interface was found to cause significant atomic displacements of up to 10% of the lattice constant.[9] In this paper we present detailed results for the {100} interfaces, which combine polar CdTe faces with a neutral PbTe face. Comparison is made to reported results of the same structural type of interface in the ErAs/InGaAs heterosystem.

The two tellurides PbTe and CdTe differ fundamentally in their bonding configurations [Fig. 2(a)]. PbTe consists of group-IV and group-VI atoms with strong ionic bonds. Each atom in this *rs* structure has six nearest neighbors and the two elements occupy two face-centered-cubic (fcc) sublattices displaced by (1/2, 1/2, 1/2) of the cubic lattice constant a_0. The more covalent II-VI compound CdTe has a *zb* crystal structure and fourfold coordinated atoms, which occupy fcc

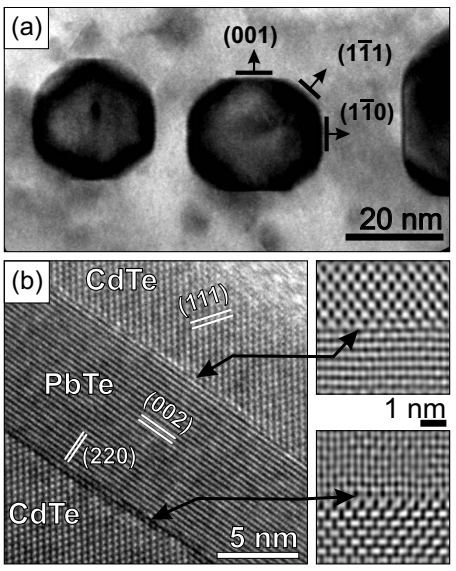

FIG. 1. (a) TEM image of coherently precipitated PbTe QDs with the three characteristic interfaces. (b) HRTEM images of opposite interfaces of a PbTe SQW embedded in CdTe. Clearly visible are the distinctively different symmetry-allowed lattice fringes (002) and (220) in *rs*—PbTe, and (111) and ($\bar{1}\bar{1}$1) in *zb*—CdTe.

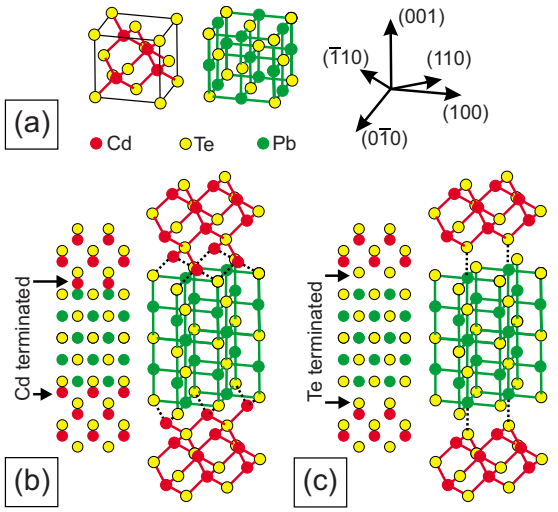

FIG. 2. (Color online) (a) Stick-and-ball representation of the bonding configurations of *rs*—PbTe and *zb*—CdTe. 3D and projected representations of the atoms in a CdTe/PbTe/CdTe heterostructure with both interfaces (b) Cd terminated, or (c) Te terminated. The geometry represents the experimental situation with growth along (001) and TEM images recorded along a ⟨110⟩ zone axis.

sublattices that are displaced by $(1/4,1/4,1/4)a_0$. The room-temperature lattice constants of the two materials differ by just 0.3% (a_{PbTe}=0.6462 nm and a_{CdTe}=0.6481 nm), which allows almost strain-free growth of the heterostructure. The (001) face of the *rs* lattice is nonpolar, and thus the cleavage plane, whereas *zb* has two different polar (001) planes, which are either cation [Cd: (001)A] or anion [Te: (001)B] terminated. With a continuous fcc matrix of the common Te atoms,[9] the (001) interface in a *rs*/*zb* heterostructure results in two possible atomic arrangements, which were referred to in the literature as "chain" and "shadow" configurations.[10] In both models the continuous Te fcc matrix is filled with Pb and Cd fcc sublattices in the PbTe- and CdTe-crystal halves, respectively. It is the termination of the CdTe half that defines the kind of the interface model. The chain model corresponds to the Cd-terminated (001)A interface [Fig. 2(b)], in which the CdTe zigzag chains of the CdTe half extend across the interface, where they become terminated by the Te atoms of the first PbTe lattice plane. The shadow model [Fig. 2(c)] corresponds to the situation where the CdTe half is Te terminated and therefore the Pb atoms of the first PbTe lattice plane are located above the Te atoms of the CdTe-crystal half. The two possible atomic arrangements lead to different lattice-plane spacings at the nominal position of the interface: The Cd-terminated (001)A interface assumes the CdTe lattice-plane spacing along [001], namely $1/4a_0$, whereas the lattice-plane spacing for the Te-terminated (001)B interface is that of PbTe along [001], i.e., $1/2a_0$. In addition, the [110] and [$\bar{1}$10] zone axes are not equivalent and lead to different interface appearances in the projection of the atoms onto the respective plane. Although the same coordinate system is used for all parts of Fig. 2, the nonequivalence of the [110] and [$\bar{1}$10] zone axes is still visualized, by plotting in Figs. 2(b) and 2(c), respectively,

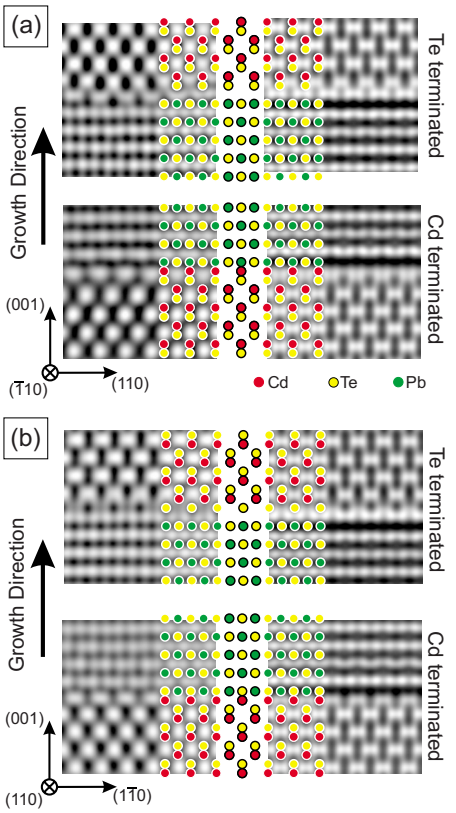

FIG. 3. (Color online) Comparison of HRTEM images (left) with HR simulations (right) for the four possible combinations of interface termination and zone axes. The stick-and-ball models identify the atomic positions derived from the respective simulations.

three-dimensional (3D) representations and projections of CdTe/PbTe/CdTe slabs with the same termination type on the lower and upper interface. The different stacking orders at the two interfaces are equivalent to two orthogonal ⟨110⟩ zone axes applied to the same stacking order, as shown in Fig. 3. The considerations regarding (001)A and (001)B interfaces, and the different ⟨110⟩ zone axes apply generally to any (*rs*)/(*zb*) material system with a continuous sublattice throughout the interface, including the ErAs/$In_{1-x}Ga_xAs$ heterosystem.[10,11]

Recently, first observations of both (001)A and (001)B interface types became known for PbTe/CdTe,[9] whereas in growth experiments of ErAs on $In_{1-x}Ga_xAs$ so far only the (001)A interface has been reported in the literature.[11] The PbTe/CdTe system is particularly well suited for investigations of both interfaces because 2D PbTe layers with sharp interfaces on either side can be embedded in a CdTe host[7,8,12] via low-temperature molecular-beam epitaxy (MBE), as shown in Fig. 1(b). In addition, QDs resulting from such 2D PbTe layers by precipitation during thermal annealing can be size tuned via the thickness of the original PbTe layer.[12] Such QD precipitates develop their interfaces during a substantial shape transformation via solid-state diffusion and are thus close to the thermal equilibrium state. They also become readily accessible by HRTEM interfaces studies because it is much easier to realize specimen thicknesses smaller than or

TABLE I. List of specimens used in this study. Specimens with the same number are from the same epitaxial sample. Termination (Cd or Te) refers to the surface of the CdTe pseudosubstrate; status stands for as-grown single-quantum wells (G), or for quantum dots induced by thermal annealing (A). The two nonequivalent zone axes [110] and [$\bar{1}$10] were determined on the specimen pair 31a and 31b, and subsequently assigned to the other specimens.

Specimen	Termination	Growth temp. (°C)	Status	Zone axis
5	Cd	250	G	[110]
8a	Te	280	G	[110]
8b	Te	280	A	[110]
11	Cd	280	A	[$\bar{1}$10]
12	Te	280	A	[$\bar{1}$10]
31a	Cd	220	A	[110]
31b	Cd	220	A	[$\bar{1}$10]

comparable to the diameter of the relatively large PbTe QDs (typically >10 nm) than is the case for ErAs dots in $In_{1-x}Ga_xAs$ with typical diameters <2 nm.[5]

Table I lists the CdTe/PbTe heterostructures employed for this study. The samples were grown by MBE on CdTe buffers on top of semi-insulating (001)-GaAs substrates.[13] By changing the growth conditions from Cd rich to Te rich, the surface of the CdTe buffer becomes either Cd or Te terminated and thus allows the investigation of the {001} interfaces with either excess Cd or Te atoms at the first interface of the growth sequence.[14] Subsequently, single PbTe quantum wells (SQWs) with different thicknesses were grown at temperatures ranging from 220 to 250 °C and then capped with 50 nm of CdTe. The samples were either investigated as grown (labeled "G" in Table I) or after a transformation of the SQWs into PbTe QDs, which was induced by post growth annealing at $\geq$300 °C for 10 min in an inert-gas atmosphere (labeled "A" in Table I).

The structures were investigated by HRTEM with a JEOL 2011HR FasTEM instrument operated at 200 keV in the dedicated high-resolution mode with small convergence angle. The images were recorded with a Gatan Multiscan camera on cross-sectional specimens along ⟨110⟩ zone axes. In this geometry the structure factors of the *zb*-CdTe lattice allow only {111} diffraction, whereas {002} and {220} spots are symmetry allowed in the *rs*-PbTe lattice. Only the lattice fringes associated with the allowed reflexes are observable in HRTEM images. This greatly simplifies the discrimination between the two lattice types, as shown in Fig. 1(b). The extinction lengths along the crystallographic directions of the dominant diffraction reflexes are on the order of 38–58 nm at 200 keV. For an easy interpretation of the phase-contrast HRTEM images the specimen thickness had to be thinned to below the excitation length. Specimen preparation was based on mechanical dimple grinding, followed by shallow-angle Ar-ion sputtering in a Gatan PIPS apparatus. Because of the aforementioned nonequivalence of the ⟨110⟩ zone axes, a specimen pair was prepared from sample 31 (Table I) to allow imaging along two orthogonal ⟨110⟩ directions. The actual zone axes of the other specimens were determined by comparison with the TEM images of specimen pair 31 and are also listed in Table I.

Under ideal defocusing conditions the spacings of the lattice fringes are directly correlated with the respective lattice-plane spacings of the crystals. Nevertheless, HR map simulations are necessary for an unequivocal interpretation of phase-contrast HRTEM images, especially in the presence of interfaces. HR image simulations were performed with the commercial JEMS software package[15] which is based on the dynamical theory of small-angle elastic electron diffraction in a multislice approach. Adjustable parameters are specimen thickness and defocusing conditions, in addition to the lens aberration parameters of the TEM instrument.

A fundamental question is the kind of termination at opposite CdTe/PbTe (001) interfaces. Generally, one might expect different terminations at opposite (001) faces for reasons of stochiometry preservation but if the interface energies are too different, local violation of stochiometry might lead to an overall lower-energy configuration with the lower-energy face developing on both interfaces. Such a configuration has indeed be suggested for the ErAs/$In_{1-x}Ga_xAs$ heterostructure.[11] To address this problem in the PbTe/CdTe system, we compared HRTEM images recorded both at as-grown PbTe layers and at dots formed by annealing, with HR simulations. All PbTe layers had a nominal thickness in the range of 3–5 nm. CdTe buffers with either Te and Cd termination were employed as substrates for PbTe growth. Because of the rather large number of samples investigated (Table I), we were able to record complete sets of opposite {001} interfaces at dots as well as on SQWs for both buffer terminations.

The interfaces were imaged as defocus series around the Scherzer-defocus condition, where the resolution limit is achieved. Moreover, under these conditions the phase contrast does not change sign for lattice spacings above the resolution limit. HRTEM images near the Scherzer defocus were subsequently compared with the HR simulations. The most distinctive feature of the Cd- and the Te-terminated interfaces is the lattice-plane spacing at the interface. In the former case an additional Cd lattice plane is inserted between the PbTe and the CdTe-crystal halves [Fig. 2(b)]. This leads for the Te- (Cd-)terminated interface to a spacing above (below) the resolution limit of our microscope, which allows a clear discrimination between (001)A and (001)B.

Results are shown in Fig. 3, where both interface terminations and the two nonequivalent ⟨110⟩ zone axes are depicted. In each frame HRTEM images are shown to the left, the corresponding simulations to the right, and stick-and-ball atomic configurations are plotted in between. Dark areas in the images and simulations correspond to atomic positions. For the Te-terminated interfaces, the lattice fringes associated with the two crystal halves are clearly separated, whereas an overlap of the lattice fringes occurs in the case of the Cd-terminated interface.

To speed up interface identification and to find qualitative evidence for the conformity of the HRTEM image with the simulations, we developed a semiautomatic algorithm. It is based on a comparison of the autocorrelation function of the HRTEM image with the cross-correlation function of HR-

TABLE II. Calculated chemical potentials and resulting formation enthalpies of the considered materials in (eV). For more details see Ref. 20.

$\mu_{\mathrm{In}}^{\mathrm{bulk}}$	$\mu_{\mathrm{Ga}}^{\mathrm{bulk}}$	$\mu_{\mathrm{As}}^{\mathrm{bulk}}$	$\mu_{\mathrm{InGaAs_2}}^{\mathrm{bulk}}$	$\mu_{\mathrm{Cd}}^{\mathrm{bulk}}$	$\mu_{\mathrm{Te}}^{\mathrm{bulk}}$	$\mu_{\mathrm{CdTe}}^{\mathrm{bulk}}$	$\Delta H_f^{\mathrm{InGaAs_2}}$	$\Delta H_f^{\mathrm{CdTe}}$
−3.17	−3.64	−5.39	−18.53	−1.55	−3.87	−6.33	0.94	0.91

TEM and simulated image. This allows an immediate identification of the zone axis and a greatly simplified assignment of the interface termination. As a general result, we found that both on SQWs and dots opposite PbTe/CdTe(001) interfaces have different terminations. Moreover, the type of the first interface in growth direction is always determined by the buffer termination before PbTe growth. Among the large number of investigated interfaces we found only very few cases, where seemingly the same termination on opposite faces was observed. Closer inspection revealed that such rare events occur only in the presence of crystallographic defects such as stacking faults.

To clarify, why the structural and electronically similar heterosystems PbTe/CdTe and ErAs/$In_{1-x}Ga_xAs$ develop seemingly different {001} interfaces, first-principles total-energy calculations were performed. We applied the density-functional theory (DFT) within the local-density approximation (LDA) as implemented in the Vienna *ab initio* simulation package (VASP).[16,17] More details regarding the simulations in the repeated slab approximation are described for PbTe/CdTe in Refs. 9, 18, and 19, and for ErAs/InGaAs in Ref. 20

The repeated slab approximation yields an interface energy averaged over opposite interfaces. It corresponds to the interface-formation energy per interface area A_{int},

$$\gamma^{\mathrm{form}} = \frac{1}{2A_{\mathrm{int}}}\left[E_{\mathrm{tot}}(\mathrm{int}) - \sum_a N_a \mu_a\right],$$

assuming that the interface is formed by atoms from reservoirs with the chemical potentials μ_a. Thereby, the total number of atoms of type a is denoted by N_a and E_{tot}(int) corresponds to the total energy of the system. Under thermal equilibrium conditions the sum of the chemical potentials of the interface atoms is equal to the chemical potential of the corresponding bulklike material layers which serve as atomic reservoirs, e.g., $\mu_{\mathrm{Cd}}+\mu_{\mathrm{Te}}=\mu_{\mathrm{CdTe}}^{\mathrm{bulk}}$. On the other hand, the chemical potential of a bulk material is equal to

$$\mu_{\mathrm{CdTe}}^{\mathrm{bulk}} = \mu_{\mathrm{Te}}^{\mathrm{bulk}} + \mu_{\mathrm{Cd}}^{\mathrm{bulk}} - \Delta H_f^{\mathrm{CdTe}},$$

where $\Delta H_f^{\mathrm{CdTe}}$ is the formation enthalpy of bulk CdTe. Taking into account that the chemical potential at the interface has to be smaller than that of the bulk phase $\mu_a \leq \mu_a^{\mathrm{bulk}}$ with $a \in \{\mathrm{Cd}, \mathrm{Te}\}$ (otherwise the material would condensate in its bulk phase), we obtain a finite codomain

$$-\Delta H_f^{\mathrm{CdTe}} \leq \Delta\mu_{\mathrm{Te}} = \mu_{\mathrm{Te}} - \mu_{\mathrm{Te}}^{\mathrm{bulk}} \leq 0.$$

The same argumentation can be applied to the In or Ga atoms at ErAs/InGaAs interfaces

$$-\Delta H_f^{\mathrm{InGaAs}} \leq \Delta\mu_{\mathrm{In}}, \quad \Delta\mu_{\mathrm{Ga}} \leq 0.$$

The calculated values[20] for the corresponding formation enthalpies and chemical potentials can be found in Table II.

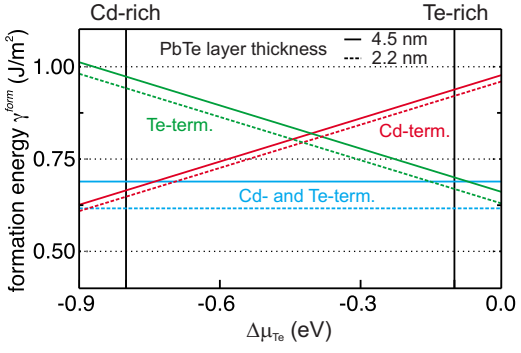

FIG. 4. (Color online) Interface-formation energy γ^{form} vs the relative abundance of Te atoms, which is represented by the chemical potential $\Delta\mu_{\mathrm{Te}}$. The line pairs stand for different terminations at opposite interfaces (horizontal lines and blue online), complete Cd termination (inclining and red online), and complete Te termination (declining and green online). Solid and dashed lines are results for two different PbTe layer thicknesses, as indicated.

The results for the interface-formation energy of CdTe/PbTe are shown in Fig. 4. Here γ^{form} is plotted versus the change in the chemical potential $\Delta\mu_{\mathrm{Te}}$ of Te interface atoms. The left-hand side of the panel corresponds to Cd rich and the right-hand side to Te-rich growth conditions. The flat line pair represents different terminations at opposite interfaces, the inclined line pair represent Cd termination at both interfaces, and declining lines stand for complete Te termination. Solid lines are for a PbTe slab thickness of 4.5 nm and dashed lines for a thickness of 2.2 nm. In agreement with the experimental findings, different terminations at opposite interfaces are energetic most favorable. Only under extremely Cd- or Te-rich conditions, the same interface type is predicted to occur on either side of the PbTe slab. The range of $\Delta\mu_{\mathrm{Te}}$, where opposite interface terminations are energetically favorable, becomes narrower with increasing PbTe layer thickness. The origin of this thickness dependence lies in the strong polarity of the CdTe bonds in combination with dielectric screening in the PbTe slab. The former leads to a pronounced charge density at the first interface, which affects the development of the second interface during growth in such a way that overall charge neutrality, and thus stochiometry, is preserved. With increasing thickness of the PbTe layer, its rather high dielectric constant ($\varepsilon_{\mathrm{PbTe}}$=32) (Ref. 21) leads to more and more pronounced electrostatic decoupling of the two interfaces. For large thicknesses one would therefore expect independent development of the interfaces, which then should only depend on the growth conditions, i.e., on $\Delta\mu_{\mathrm{Te}}$.

The same type of stability analysis was also applied to

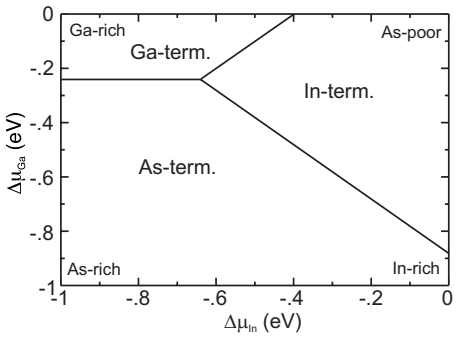

FIG. 5. Phase diagram for the stability of different interfaces in $ErAs/In_{1-x}Ga_xAs$ as a function of the chemical potentials $\Delta\mu_{Ga}$ and $\Delta\mu_{In}$. Only interfaces with the same termination on opposite faces were found to be stable.

$ErAs/In_{1-x}Ga_xAs$. For this system we found in thermodynamic equilibrium under no conditions of the chemical potentials $\Delta\mu_{Ga}$ and $\Delta\mu_{In}$ oppositely terminated interfaces in the slab. That is, opposite interfaces are terminated by Ga-Ga, In-In (Type-A), or As-As (Type-B) faces, depending only on the relative abundances of Ga and In atoms during interface formation, which are described by their respective chemical potentials. This result is depicted in Fig. 5 as a phase diagram that shows the areas, where each of the interface pairs is stable.

Within this model description, the underlying mechanism for $ErAs/In_{1-x}Ga_xAs(001)$ interface formation follows the same rationale as discussed for the PbTe/CdTe heterosystem. In contrast to the II-VI compound CdTe, however, the bonds in the III-V compound $In_{1-x}Ga_xAs$ are much less polar whereas screening in the semimetal ErAs is similarly effective ($\varepsilon_{ErAs} \approx 25$) (Ref. 6) as in PbTe. The much weaker interface dipole is therefore already screened for thin layers (4.5 nm in Fig. 5), which effectively decouples the interfaces under most experimentally accessible conditions. The interface termination is thus expected to be just determined by the relative abundance of the constituents during interface formation.

While the result of the *ab initio* calculations for PbTe/CdTe are fully consistent with our experimental findings, the predictions for the $ErAs/In_{1-x}Ga_xAs(001)$ interfaces require more careful discussion, as they appear to contradict to some extent the experimental results in Ref. 11: there, Klenov *et al.* investigated the (001) interface between a GaAs substrate and an ErAs layer, which was grown epitaxially under As-rich growth conditions. They found a Ga-terminated (001)A interface and came to the tentative conclusion that the chain configuration of the (001)A interface is energetically most favorable. In contrast, the results of our *ab initio* calculations in Fig. 5 would suggest that both As-terminated (001)B interfaces and Ga-terminated (001)A interfaces can occur under As-rich and Ga-rich conditions, respectively. This seeming inconsistency can be resolved, when taking into account the recent experimental results of Schultz and Palmstrøm,[22] who found a self-embedding mechanism for ErAs on GaAs(001). Their interpretation of the experiments is based on the substantially different formation enthalpies of ErAs and GaAs, which lead to a replacement of Ga atoms in the topmost layers of the substrate by Er atoms from the growth process. This self-embedding mechanism becomes limited after a few atomic layers by diffusion of subsequent Er atoms through the already formed regions of *rs* ErAs. On the other hand, the replaced Ga atoms have to diffuse in opposite direction through the ErAs regions to the surface, where they can form GaAs with the As surplus provided by As-rich growth conditions.[22] Such an interface-formation mode, which resembles to some extent the thermal oxidation of Si, can readily be reconciled with our *ab initio* results. The formation of the buried ErAs/GaAs(001) interface becomes effectively decoupled from the epitaxial growths conditions at the surface, which are in most experiments As rich because of the high vapor pressure of As. Instead, the buried interface forms under Ga-rich conditions, which are created by the replaced Ga atoms diffusing toward the surface. Therefore, a Ga-terminated (001)A interface can be expected, as has indeed been observed experimentally.[11] However, this does not mean, as was suggested in Ref. 11, that the chain configuration itself is energetically more favorable. Instead, the chemical potential $\Delta\mu_{Ga}$ determines which of the two interface configurations actually develops. Because of the proposed self-embedding mechanism one would always expect the (001)A configuration at the first ErAs/Ga(In)As interface in growth direction but the second interface could as well become As terminated if grown under As-rich conditions. To test this prediction of the *ab initio* calculations, HRTEM images of the second interface are required, which, to our knowledge, have not been reported as yet.

In summary, we showed that PbTe embedded in CdTe forms SQWs or QDs with coherent {001} interfaces. In the absence of crystallographic defects, we always found local stochiometry preserved, i.e., PbTe SQW as well as dots are terminated by (001)A and (001)B interfaces on opposite sides. The termination of the first interface in growth direction determines the stacking order of the interfaces and can be controlled by the epitaxial-growth conditions of the CdTe buffer layer. This behavior was confirmed by *ab initio* calculations, and is attributed to the strong ionic bonding character of the II-VI compound CdTe, which leads to the formation of a pronounced interface dipole. In contrast, the much less ionic bonds in $In_{1-x}Ga_xAs$ together with the effective dielectric screening in the embedded ErAs semimetal layer lead to decoupling of the two interfaces, which tend to develop a termination that is entirely determined by the relative abundances of anions and cations in the environment of the interface. With the recently discovered self-embedding mechanism of ErAs into a GaAs substrate via a Er/Ga replacement reaction, Ga-rich conditions can always be expected for the first interface, which is consistent both with our prediction of the (001)A interface and the experimental observations in Ref. 11. It remains to be seen if the second interface can become As terminated if grown under As-rich conditions, as predicted by our calculations.

This work was supported by the Austrian science foundation FWF via the projects SFB 025: IRON and START Y179. In addition grants of computer time from the HLRS Stuttgart and the LRZ Munich are gratefully acknowledged.

*Corresponding author; friedrich.schaffler@jku.at

[1] C. J. Palmstrøm, N. Tabutabaie, and A. J. Allen, Appl. Phys. Lett. **53**, 2608 (1988).
[2] Hae-Kyung Jeong, Takashi Komesu, Cheol-Soo Yang, P. A. Dowben, B. D. Schultz, and C. J. Palmstrøm, Mater. Lett. **58**, 2993 (2004).
[3] N. G. Stoffel, C. J. Palmstrøm, and B. J. Wilkens, Nucl. Instrum. Methods Phys. Res. B **56-57**, 792 (1991).
[4] C. Kadow, S. B. Fleischer, J. P. Ibbetson, J. E. Bowers, A. C. Gossard, J. W. Dong, and C. J. Palmstrøm, Appl. Phys. Lett. **75**, 3548 (1999).
[5] D. O. Klenov, D. C. Driscoll, A. C. Gossard, and S. Stemmer, Appl. Phys. Lett. **86**, 111912 (2005).
[6] E. R. Brown, A. Bacher, D. Driscoll, M. Hanson, C. Kadow, and A. C. Gossard, Phys. Rev. Lett. **90**, 077403 (2003).
[7] W. Heiss, H. Groiss, E. Kaufmann, G. Hesser, M. Böberl, G. Springholz, F. Schäffler, K. Koike, H. Harada, and M. Yano, Appl. Phys. Lett. **88**, 192109 (2006).
[8] W. Heiss, H. Groiss, E. Kaufmann, G. Hesser, M. Böberl, G. Springholz, F. Schäffler, R. Leitsmann, F. Bechstedt, K. Koike, H. Harada, and M. Yano, J. Appl. Phys. **101**, 081723 (2007).
[9] R. Leitsmann, L. E. Ramos, F. Bechstedt, H. Groiss, F. Schäffler, W. Heiss, Kazuto Koike, Hisahsi Harada, and Mitsuaki Yano, New J. Phys. **8**, 317 (2006).
[10] E. Tarnow, J. Appl. Phys. **77**, 6317 (1995).
[11] D. O. Klenov, J. M. Zide, J. D. Zimmerman, A. C. Gossard, and S. Stemmer, Appl. Phys. Lett. **86**, 241901 (2005).
[12] H. Groiss, E. Kaufmann, G. Springholz, T. Schwarzl, G. Hesser, F. Schäffler, W. Heiss, T. Koike, T. Itakura, T. Hotei, M. Yano, and T. Wojtowicz, Appl. Phys. Lett. **91**, 222106 (2007).
[13] K. Koike, T. Tanaka, S. Li, and M. Yano, J. Cryst. Growth **227–228**, 671 (2001).
[14] K. Koike, T. Honden, I. Makabe, F. P. Yan, and M. Yano, J. Cryst. Growth **257**, 212 (2003).
[15] http://cimewww.epfl.ch/people/stadelmann/jemsWebSite/jems.html
[16] G. Kresse and J. Furthmüller, Comput. Mater. Sci. **6**, 15 (1996).
[17] G. Kresse and J. Furthmüller, Phys. Rev. B **54**, 11169 (1996).
[18] R. Leitsmann and F. Bechstedt, Phys. Rev. B **76**, 125315 (2007).
[19] R. Leitsmann and F. Bechstedt, Phys. Rev. B **78**, 205324 (2008).
[20] R. Leitsmann, Ph.D. thesis, Universität Jena, 2009.
[21] C. Kittel, *Introduction to Solid State Physics* (Wiley, New York, 1976), pp. 308–309.
[22] B. D. Schultz, C. J. Palmstrøm, Phys. Rev. B **73**, 241407(R) (2006).